Available online at www.sciencedirect.com
ScienceDirect
Ceramics International 35 (2009) 1195–1204
CERAMICS INTERNATIONAL
www.elsevier.com/locate/ceramint

In vitro behavior of bioactive phosphate glass–ceramics from the system P_2O_5–Na_2O–CaO containing titania

H.A. ElBatal [a], E.M.A. Khalil [b], Y.M. Hamdy [b,*]

[a] *Glass Research Department, National Research Center, Dokki, Cairo, Egypt*
[b] *Spectroscopy Department, National Research Center, Dokki, Cairo, Egypt*

Received 14 February 2008; received in revised form 21 April 2008; accepted 12 June 2008
Available online 16 July 2008

Abstract

Soda lime phosphate bioglass–ceramics with incorporation of small additions of TiO_2 were prepared in the metaphosphate and pyrophosphate region, using an appropriate two-step heat treatment of controlled crystallization defined by differential thermal analysis results. Identification and quantification of crystalline phases precipitated from the soda lime phosphate glasses were performed using X-ray diffraction analysis. Calcium pyrophosphate (β-$Ca_2P_2O_7$), sodium metaphosphate ($NaPO_3$), calcium metaphosphate (β-$Ca(PO_3)_2$), sodium pyrophosphate ($Na_4P_2O_7$), sodium calcium phosphate ($Na_4Ca(PO_3)_6$) and sodium titanium phosphate ($Na_5Ti(PO_4)_3$) phases were detected in the prepared glass–ceramics. The degradation of the prepared glass–ceramics was carried out for different periods of time in simulated body fluid at 37 °C using granules in the range 0.300–0.600 mm. The released ions were estimated by atomic absorption spectroscopy and the surface textures were measured by scanning electron microscopy. Investigation of in vitro bioactivity of the prepared glass–ceramics was done by the measurement of the infrared reflection spectra for the samples after immersion in the simulated body fluid for different periods at 37 °C. The result showed that no apatite layer was formed on the surface of the samples and the dominant phase remained on the surface was β-$Ca_2P_2O_7$, which is known for its bioactivity.

Keywords: B. Spectroscopy; C. Corrosion; D. Glass ceramics; E. Biomedical applications

1. Introduction

Bioactive glasses and glass–ceramics are of great interest for medical applications due to their osteoconductive and osteoinductive properties. Various types of bioactive materials have been developed over the last three decades [1–3]. The main bioactive glasses, glass–ceramics and ceramics used clinically are bioglass in the system Na_2O–CaO–SiO_2–P_2O_5, hydroxyapatite (HA) $Ca_{10}(PO_4)_6(OH)_2$, β-tricalcium phosphate (TCP) $Ca_3(PO_4)_2$, HA/TCP bi-phase ceramics and glass–ceramics A–W containing crystalline oxyfluoroapatite [($Ca_{10}(PO_4)_6O$, F) and β-wollastonite ($CaOSiO_2$) in an MgO–CaO–SiO_2 glassy matrix].

Most of the published works on bioactive glasses and glass–ceramics are concentrated on SiO_2-based materials. However, there is uncertainty about the long-term effect of silicon in vivo. The use of crystalline phosphate ceramics has attracted much recent interest to the development of phosphate glasses and glass–ceramics for use in orthopaedic implants because their chemical and physical properties make them suitable for use as bone-binding materials.

Vogel and Holand [4] prepared resorbable bioglass–ceramics from the system Na_2O–CaO–P_2O_5 with some Al_2O_3 to control the dissolution rate. After special thermal treatment, some crystalline phases were separated and implantation experiments demonstrated that the bone substance grows into the phosphate glass–ceramics without the formation of connective tissues. Alkemper and Fuess [5] studied the crystallization of the same system without nucleating agent and showed that the addition of fluorine does not basically affect the nucleation mechanism, but the ranges of nucleation and crystal growth overlap. Uo et al. [6] studied the cytotoxicity of Na_2O–CaO–P_2O_5 glasses upon dissolution in water or simulated body fluid. Kasuga et al. [7,8] prepared and studied extensively calcium phosphate glass–ceramics with different additives (MgO, TiO_2, etc.) and compared their bioactivity.

In this work, some selected bioglasses from the system Na_2O–CaO–P_2O_5 with some additions of TiO_2 were prepared

* Corresponding author.
E-mail address: yousry_m_h@yahoo.com (H.A. ElBatal).

0272-8842/$34.00
doi:10.1016/j.ceramint.2008.06.004

and then converted to the corresponding bioglass–ceramics by controlled two-step thermal heat treatment. The objectives of this work were to: (1) characterize some phosphate-based bioglasses and their corresponding bioactive glass–ceramics and (2) evaluate the bioactivity of the prepared biomaterials in vitro.

2. Materials and methods

2.1. Glass preparation

Six glasses were prepared from chemically pure $CaCO_3$, Na_2CO_3, $NH_4H_2PO_4$ and TiO_2 (see Table 1 for their compositions). The batches were weighed out and then melted in porcelain crucibles in an electric furnace between 1100 °C and 1200 °C for 2 h and the melts were rotated two times to achieve homogeneity. Upon complete melting, the glasses were cast in a preheated stainless steel rectangular mould of the dimensions of 1 cm × 4 cm × 1 cm preheated to about 250 °C. The glass samples were transferred to an annealing muffle furnace adjusted at 350 °C and the muffle was left to cool slowly to room temperature at a rate of 25 °C/h.

2.2. Differential thermal analysis

Differential thermal analysis (DTA) measurements were carried out on powdered samples which were examined up to 700 °C using a recording DTA apparatus Setaram (France) and alumina was used as a reference material.

2.3. Preparation of glass–ceramic samples (heat treatment regime)

Based on the thermal data obtained from both dilatometric and differential thermal analysis measurements, the specific temperatures necessary for controlled thermal heat treatment regime are obtained. The heat treatment schedule consists of two-step regime, the first temperature is equivalent for efficient nucleation step and the second temperature is equivalent to the maximum crystal growth step and the two selected temperatures are generally correlated with endothermic and exothermic peaks of the DTA thermogram. For all samples, the time of holding at the first nucleation temperature was taken as 24 h to ensure maximum nuclei, while the time of the crystallization step was taken as 12 h. The two-step heat treatment regime was done in a regulated muffle furnace (Carbolite, England). The glass specimens were heated slowly to the first nucleation temperature at a rate of 3 °C/min. After holding for 24 h at the specified temperature, the muffle temperature was raised to reach the second crystallization temperature at a rate of 3 °C/min and after a second hold for 12 h, the muffle was switched off and the samples were left to cool inside the muffle to room temperature at a rate of 20 °C/h. The prepared glass–ceramic samples were polished by 600-grit paper, 1200-grit and 2500-grit silicon carbide powders and a final polish was done by cerium oxide.

Table 1
Phosphate bioglass samples compositions

Name	P_2O_5 (mol%)	CaO	Na_2O	TiO_2
P1	45	24	31.0	–
P2	45	24	30.5	0.5
P3	45	24	30.0	1.0
P4	45	24	29.5	1.5
P5	45	24	29.0	2.0
P6	45	24	28.5	2.5

2.4. Characterization of bioglass–ceramics

2.4.1. X-ray diffraction measurements

The prepared glass–ceramic samples were finely ground and the fine powder was examined using a Brukur D8 Advance X-ray diffractometer (Germany) adopting Ni-filter and Cu-target to identify the precipitated crystalline phases.

2.4.2. Microstructure measurements using scanning electron microscope

The surface textures of the prepared glass–ceramic samples were examined using a scanning electron microscope type JEOL, JXA-840A (Japan) after coating with gold using Edwards S 150A sputter coater (England).

2.4.3. Corrosion studies using atomic spectroscopy

The glass–ceramic samples, in the form of grains in the size range 0.300–0.600 mm, were subjected to the action of the simulated body fluid (SBF), prepared according to Kokubo et al. [9], at temperature of 37 °C for different periods of time. Each 0.25 g of sample grain was weighed accurately and was put in a polyethylene container. 25 ml of SBF was poured on the grains and the container was covered and put in an incubator adjusted to 37 °C. The containers were removed from the incubator at time periods 3 h, 6 h, 1 day, 3 days, 1 week and 2 weeks. Each sample was tested 3 times for each time period. The solution of SBF was filtered on ashless filter paper no. 41.

(a) Measurement of calcium, sodium, and silicon ions by atomic absorption spectroscopy (AAS): The attacking solutions were diluted with deionized water as follows: 10 times for calcium ions concentration measurement and 100 times for sodium ions concentration measurements. The SBF solution was also diluted with the deionized water and was measured with the samples. The concentration measurements for calcium, sodium ions were done on Varian Spectra AA 220 atomic absorption spectrometer with deuterium (D_2) lamp, background correction was used. Also, hollow cathode lamps were used and all the measurements were performed in the background-corrected peak-area measurement mode. The elements were determined using the flame atomic absorption spectroscopy in acetylene-air or acetylene-nitrous oxide flames.

(b) Measurement of phosphorous ions by induced coupled plasma atomic emission spectroscopy (ICP-AES): The solutions of the samples were diluted 10 times by deionized water. The SBF solution was measured with the samples. The phosphorous 214 nm spectral line was utilized for the measurements. The calibration was performed using calibration solution prepared from 1000 mg/l stock solution (Merck).

2.5. In vitro measurements of bioglass–ceramic samples

2.5.1. Surface analysis using infrared reflection spectroscopy

The polished rectangular pieces of the glass–ceramic samples were put in the simulated body fluid (SBF) at 37 °C in an incubator at static conditions, in polyethylene covered containers, for time periods of 30 min, 1 h, 2 h, 3 h, 6 h, 1 day, 3 days, 1 week and 2 weeks. The amount of SBF solution was 28 ml to achieve (surface area of sample/volume of SBF) ratio 0.1 cm. After removing the samples from the SBF at each time interval, the samples were washed with few distilled water and allowed to dry in a desiccator. The infrared reflection spectra were measured using FT-IR spectrometer (model: Jasco FT/IR-430, Japan) with diffusive reflection attachment (model DR-400c). The spectra were collected in the wavenumber range 1400–400 cm^{-1} at resolution 2 cm^{-1}.

2.5.2. Surface analysis using scanning electron microscope

The polished rectangular pieces of bioglass–ceramic samples were soaked in the simulated body fluid solution for 2 weeks at 37 °C in an incubator at static conditions in polyethylene covered containers. The volume of SBF solution was 28 ml. After removing the pieces from the solution, they were washed with few distilled water and allowed to dry in a desiccator. Then, the surfaces of the glass–ceramic samples were examined using the scanning electron microscope (SEM) type JEOL JXA-840A (Japan) after coating with gold using Edwards S150A sputter coater (England).

3. Results

3.1. Characterization of bioglass–ceramic samples

3.1.1. Differential thermal analysis

Differential thermal analysis results are shown in Figs. 1 and 2 for phosphate bioglasses. The results reveal that the nucleation and crystallization temperatures increase with the increase of TiO_2 content for the phosphate bioglasses.

3.1.2. X-ray diffraction results for bioglass–ceramics

Figs. 3 and 4 show the X-ray diffraction patterns for the phosphate bioglass–ceramic samples. Careful inspection of the diffraction patterns indicates that the peak intensities of the crystalline phases show that calcium pyrophosphate is the main crystalline phase, then both sodium metaphosphate and calcium metaphosphate are found in considerable amounts while sodium pyrophosphate and sodium calcium phosphate are found in small amounts.

The evolution of the X-ray peaks with the increase of TiO_2 content from sample P2 to sample P6 reveals that the crystalline phases of sodium metaphosphate and calcium metaphosphate decrease with the increase of TiO_2 content except in sample P5 where the peak intensities of the sodium metaphosphate phase are still high as in sample P1. The peak intensities of the crystalline phase of sodium calcium phosphate are disappeared in all the samples containing

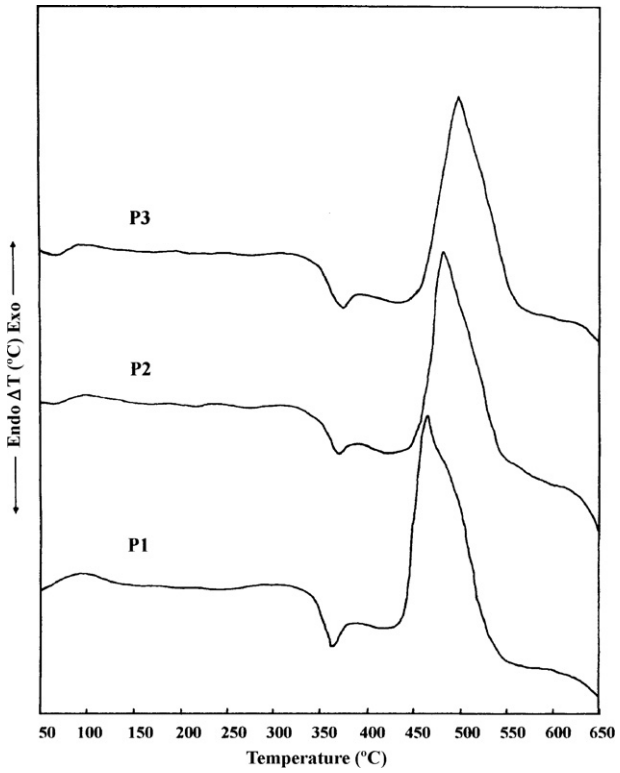

Fig. 1. Differential thermal analysis curves for the phosphate bioglass samples P1, P2, and P3 at a heating rate of 10 °C/min.

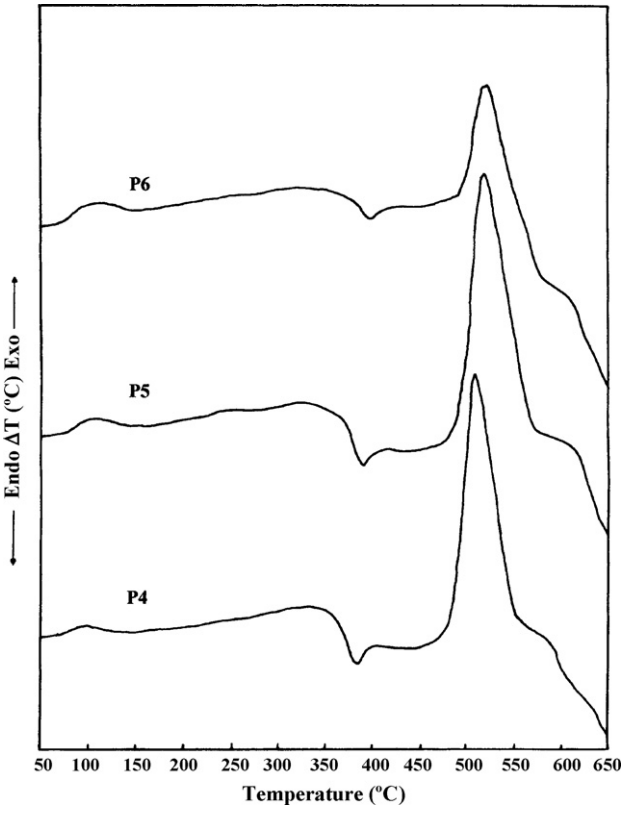

Fig. 2. Differential thermal analysis curves for the phosphate bioglass samples P4, P5, and P6 at a heating rate of 10 °C/min.

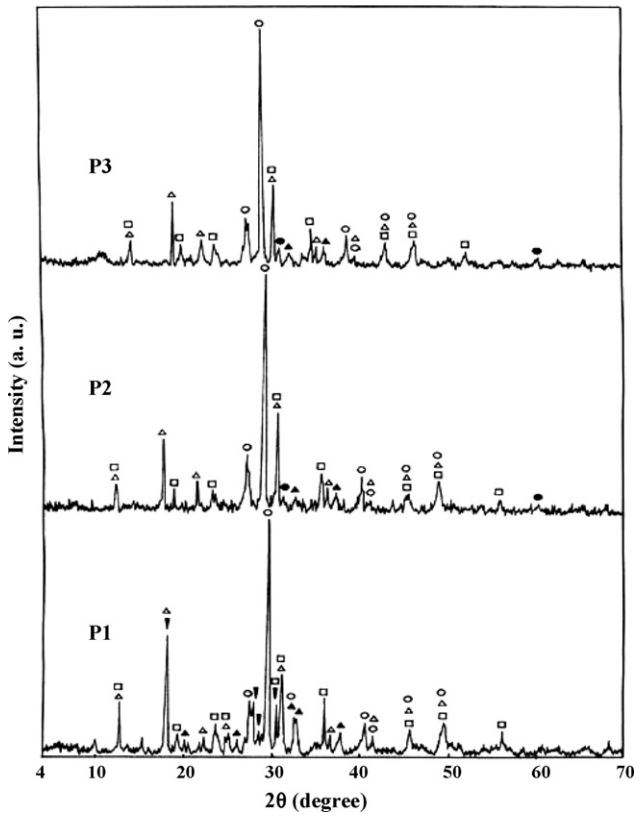

Fig. 3. X-ray diffraction patterns of the phosphate bioglass–ceramics samples (P1, P2, and P3) [(○) β-$Ca_2P_2O_7$, (△) $NaPO_3$, (□) β-$Ca(PO_3)_2$, (▲) $Na_4P_2O_7$, (▼) $Na_4Ca(PO_3)_6$, (●) $Na_5Ti(PO_4)_3$].

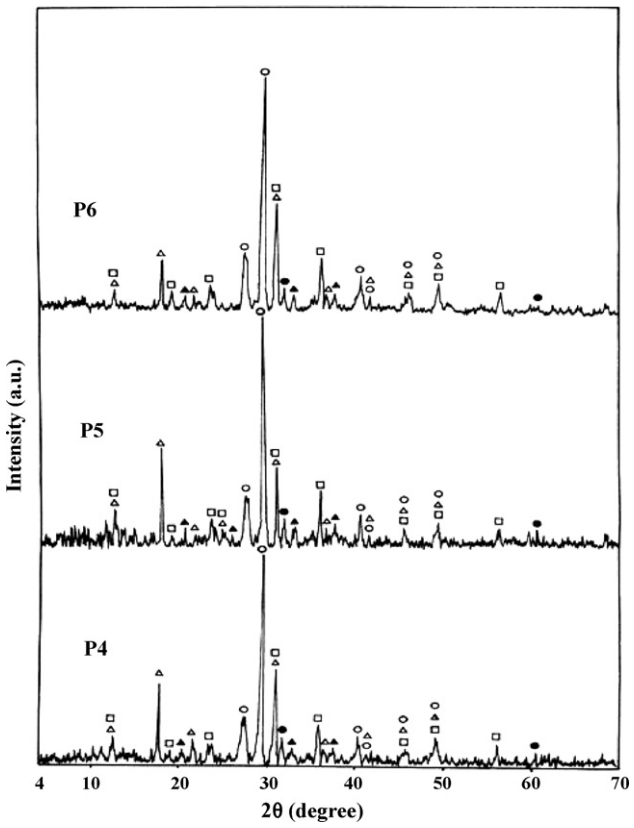

Fig. 4. X-ray diffraction patterns of the phosphate bioglass–ceramics samples (P4, P5, and P6) [(○) β-$Ca_2P_2O_7$, (△) $NaPO_3$, (□) β-$Ca(PO_3)_2$, (▲) $Na_4P_2O_7$, (●) $Na_5Ti(PO_4)_3$].

TiO_2 (P2–P6). The peak intensities of crystalline sodium pyrophosphate phase become very weak in the samples (P2–P6). With the increase of the TiO_2 content, a new phase is formed beginning from sample P2 with small peak intensities and continues to grow. The new phase is attributed to sodium titanium phosphate ($Na_5Ti(PO_4)_3$) (card number: 39-178). The peak intensities of the new-formed phase reach their maximum values in the sample P5, and then they slightly decrease in the sample P6.

3.1.3. Scanning electron microscope investigations

Fig. 5 shows the micrographs of the phosphate bioglass–ceramic samples. The morphological structure varies with the composition of the samples. All the samples show almost complete crystallization. The base glass–ceramic sample P1 shows rounded crystals of the diameter 10 μm. Increasing the TiO_2 content causes gradual decrease in the dimension of the crystals.

3.1.4. Corrosion results (elemental concentration analysis)

Fig. 6 shows the phosphorous ion concentration estimated after the immersion of the phosphate glass–ceramic samples for different reaction times. It is obvious that after 3 h of immersion, the phosphorous ion concentration sharply increases for all studied samples and with prolonged times the quantity estimated is shown to approach the double after 72 h and approaches almost saturation afterwards.

Fig. 7 shows the sodium ions concentration estimated for phosphate bioglass–ceramic samples after the immersion for prolonged times in SBF at 37 °C. The amount of released sodium ions progressively increases with time of immersion and the differences between the various bioglass–ceramic samples are small.

Fig. 8 shows the estimated calcium ions concentration released from phosphate bioglass–ceramic samples after the immersion in SBF for prolonged times at 37 °C. The bioglass–ceramics show peculiar behavior by showing a high increase of the amounts released until reaching 6 h of immersion. Further immersion, reveals a slower rate of decrease in the amounts of calcium ions.

3.2. In vitro bioactivity of bioglass–ceramic samples

3.2.1. Surface analysis using infrared reflection spectroscopy

Figs. 9 and 10 show the infrared reflection spectra of bioglass–ceramic sample P1 before and after the immersion in the simulated body fluid. The spectrum before immersion reveals peaks at 1320 cm^{-1}, 1275 cm^{-1}, shoulder at 1155 cm^{-1}, 1103 cm^{-1}, 1022 cm^{-1}, 893 cm^{-1}, 774 cm^{-1}, 742 cm^{-1}, and broad band at 666 cm^{-1}, 515 cm^{-1}.

By following the changes occurred for each peak at various reaction times, it can be shown that the peak at 1320 cm^{-1} disappeared after 3 days immersion time. The

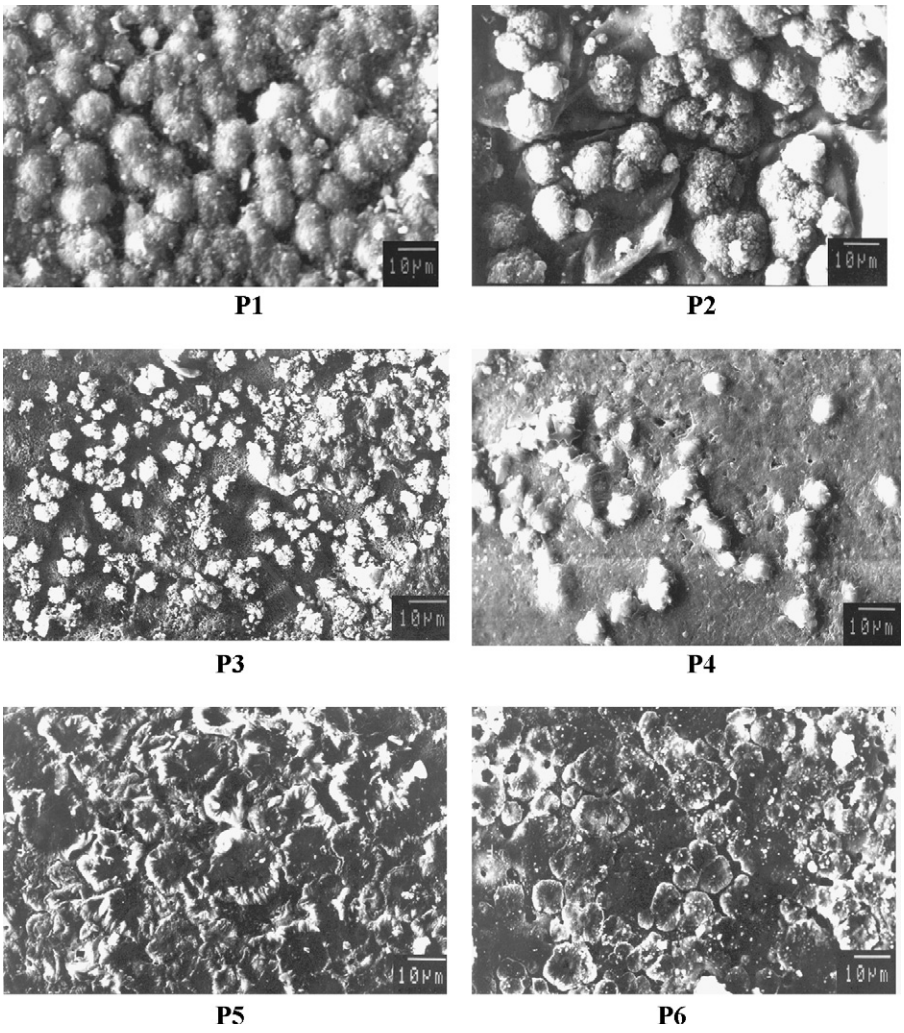

Fig. 5. Scanning electron micrographs for the bioglass–ceramic samples at magnification 1000×.

peak at 1275 cm^{-1} decreased in intensity just after 30 min of the immersion and after 6 h the peak disappeared completely. The shoulder at 1155 cm^{-1} did not change very much with time. The two peaks at 1103 cm^{-1} and 1022 cm^{-1} decreased in intensity very much after 3 h of immersion. After 6 h of immersion, the peak at 1022 cm^{-1} became less in intensity than the peak at 1103 cm^{-1}. The peak at 893 cm^{-1} did not change very much with immersion time. The band at

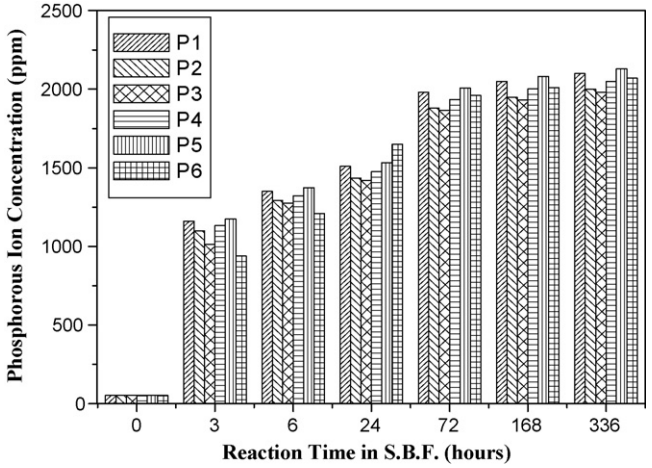

Fig. 6. Phosphorous ion concentration released from the bioglass–ceramic samples in reacted SBF after different time periods at 37 °C.

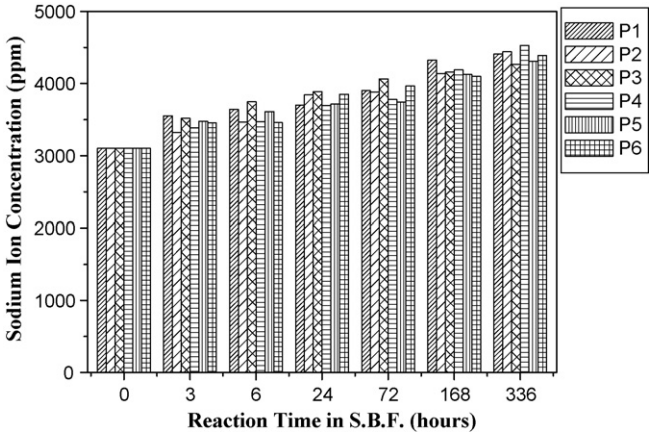

Fig. 7. Sodium ion concentration released from the bioglass–ceramic samples in reacted SBF after different time periods at 37 °C.

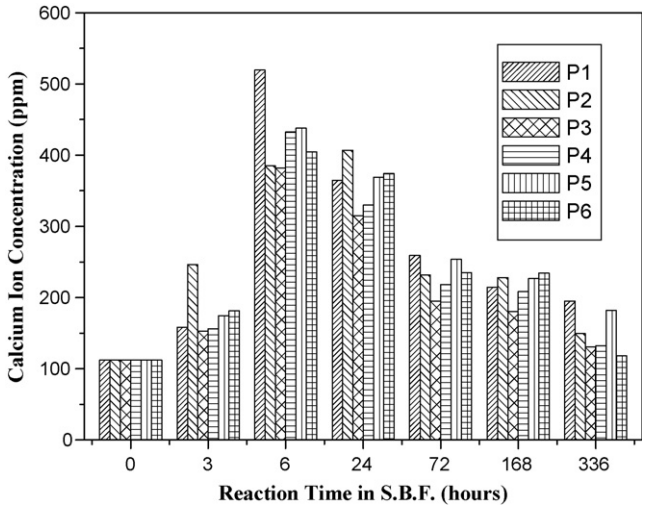

Fig. 8. Calcium ion concentration released from the bioglass–ceramic samples in reacted SBF after different time periods at 37 °C.

742 cm^{-1} decreased in intensity with time until 14 days of immersion. The 774 cm^{-1} band disappeared after 3 h of immersion time. The peak at 666 cm^{-1} decreased in intensity with time until 6 h immersion time, then it became a shoulder after 1 day and disappeared after 3 days. A new peak was

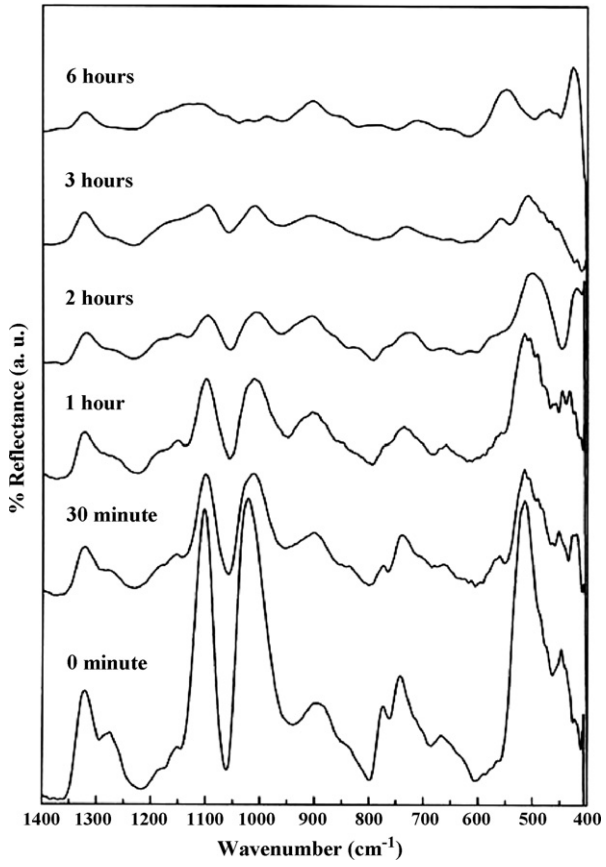

Fig. 9. Fourier transform infrared reflection spectra of the surfaces of the bioglass–ceramic sample (P1) before and after reaction with SBF for various periods.

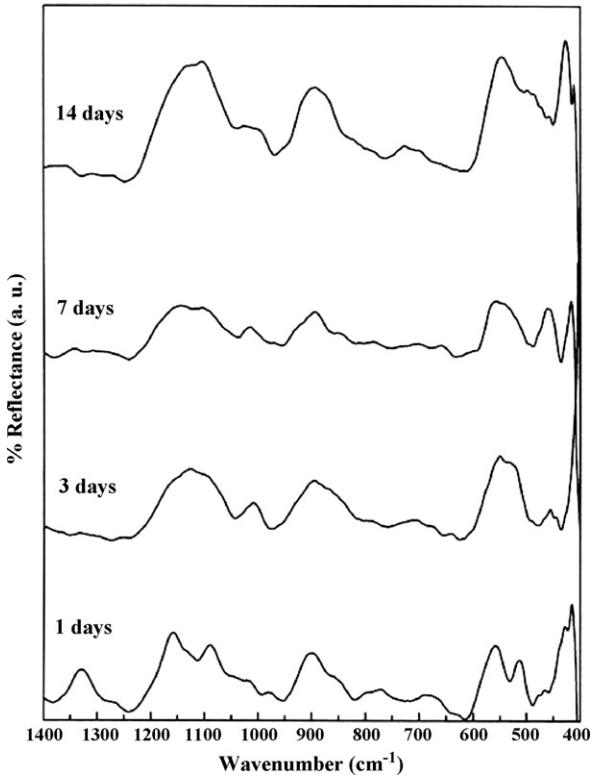

Fig. 10. Fourier transform infrared reflection spectra of the surfaces of the bioglass–ceramic sample (P1) after reaction with SBF for various periods.

formed after 30 min immersion time at 562 cm^{-1} and still existed after 3 h and then it made shift to 548 cm^{-1} after 6 h immersion time. This peak was grown by time until 14 days of immersion between 560 cm^{-1} and 548 cm^{-1}. The intensity of the peak at 515 cm^{-1} decreased with time until 14 days immersion time.

The additions of successive TiO_2 contents cause the following changes:

(a) The IR reflection spectra of sample P2 are found to be similar to sample P1.
(b) The changes observed in the IR spectra of sample P3 are those obtained from sample P1 after 6 h immersion time.
(c) The time delay for the peak intensities for sample P4 continued until 7 days immersion and after 14 days immersion, the peak intensities are similar to that for sample P1.
(d) The IR spectra of sample P5 show no change after 6 h and on reaching 14 days the spectrum resembles that of P1 after 7 days.
(e) The IR spectra of sample P6 reveal the decrease of the peak intensities after 30 min and after 7 days, the spectrum is similar to that of sample P1 after 6 h immersion.

3.2.2. Surface analysis by scanning electron microscopy

Fig. 11 shows the micrographs of the phosphate bioglass–ceramic samples after immersion in SBF for 14 days at 37 °C. All the samples did not show the formation of the apatite layer on their surfaces.

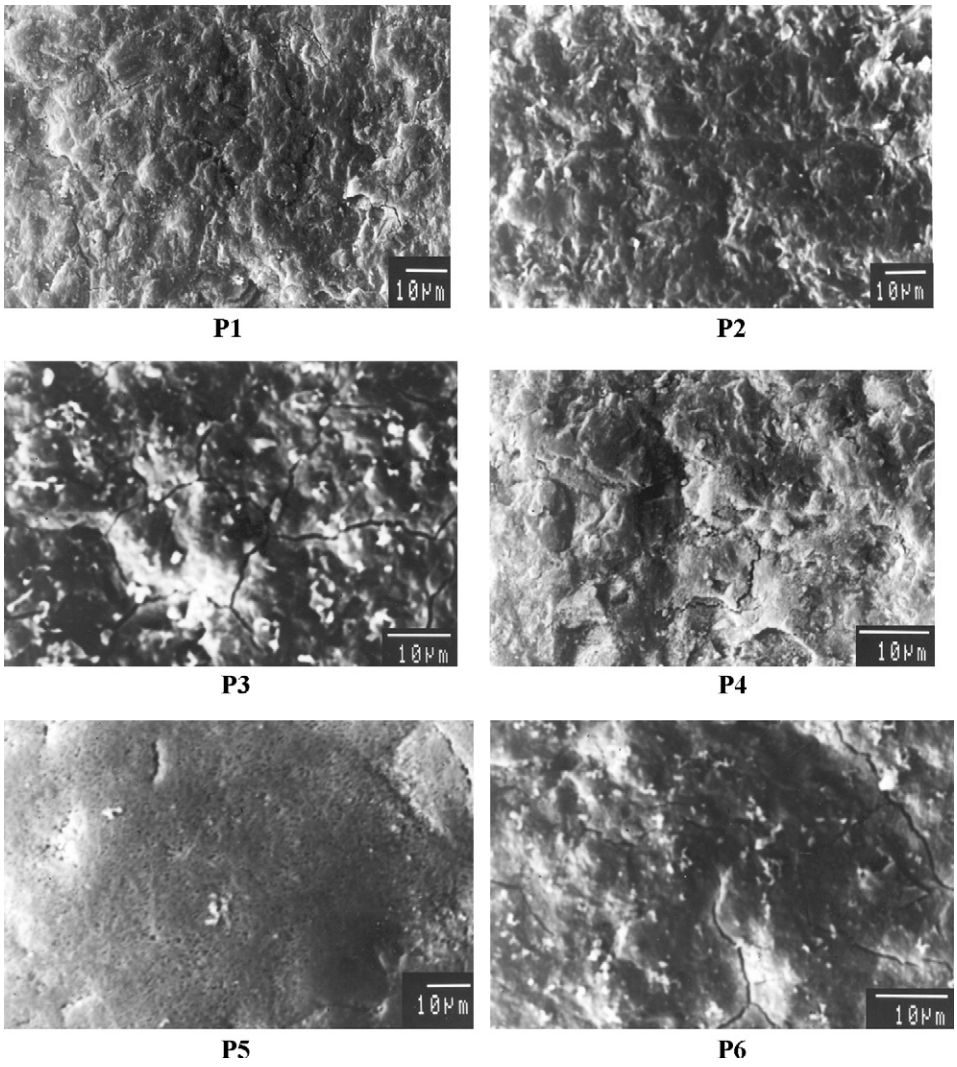

Fig. 11. Scanning electron micrographs for phosphate bioglass–ceramic samples after the immersion in SBF for 14 days at 37 °C.

4. Discussion

4.1. Differential thermal analysis measurements

Titanium oxide was assumed to form in phosphate glasses either TiO_5 or TiO_6 structural units [10]. The addition of TiO_2 to P_2O_5–CaO–Na_2O glass system leads to an increase in glass transition temperature (T_g), which can be interpreted by assuming that the titanate polyhedra forms some new interconnections within the basic phosphate structural network. The higher bonding in the structural network results in the increase of T_g values [11]. It was assumed that, when titanium cations substitute for sodium ions, $-P-O^{\delta-}\cdots Ti^{\delta+}$ bonds are formed with a strong covalent Ti–O bond than Na–O because the titanium electronegativity is larger than that of sodium [12].

From the previous assumptions, the increase of nucleation and crystallization temperatures with the addition of TiO_2 (as shown in Figs. 1 and 2) can be related to the higher bonding in the structural network. However, the increase in nucleation and crystallization temperatures with the additions of TiO_2 is not linear. This trend indicates that the incorporation of TiO_2 inside the glass network is not the same at progressive additions. This can be related to the possible different Ti–O groups with the increase of TiO_2 content. It seems that at first titanium groups may act as former oxide (TiO_5) strengthening the network and with further addition of TiO_2, the titanium oxide enters as (TiO_6) which is probably acting as modifier oxide (TiO_6).

4.2. X-ray diffraction and scanning electron microscope measurements

The X-ray diffraction pattern of the reference sample P1 (Fig. 3) indicates that the calcium pyrophosphate (β-$Ca_2P_2O_7$) is the predominant phase in the phosphate glass–ceramics. Many authors reported that the β-$Ca_2P_2O_7$ phase is formed in the glass–ceramics derived from the phosphate invert glass systems with P_2O_5 content less than 50 mol% [4,5,7,13–14].

The glasses of the system P_2O_5–CaO–Na_2O have both Q^2 (PO_2) and Q^1 (PO_3) phosphate groups. The fraction of Q^1 groups increases proportionally to the content of the network-modifying oxides, whereas the fraction of the Q^2 groups decreases [15]. The amount of the network-modifying oxides

(Na_2O and CaO) in the present system is 55 mol%, which means that the fraction of pyrophosphate groups Q^1 is high. The crystallization of this system is expected to produce also pyrophosphate and metaphosphate crystalline phases as described in the results. Franks et al. [16] reported that the sodium metaphosphate ($NaPO_3$) and sodium calcium metaphosphate ($Na_4Ca(PO_3)_6$) phases are formed in the P_2O_5–CaO–Na_2O glass system with P_2O_5 content of 45 mol%. If the Na_2O content is high, $NaPO_3$ is the major phase and if the CaO content is high, $Na_4Ca(PO_3)_6$ is the major phase and at the intermediate compositional region both phases are precipitated. It seems from the results that both phases are really precipitated but not as the major phases. However, the $NaPO_3$ phase is believed to be formed with relatively high amount after the major phase of β-$Ca_2P_2O_7$. The $Na_4Ca(PO_3)_6$ phase seems to be formed with little amount. This is consistent with the composition of N_2O content is 31 mol% and CaO content is 24 mol%.

The effect of TiO_2 addition on the crystallization process (Figs. 3 and 4) is quietly observed even with the addition of 0.5 mol% TiO_2. First, the peaks of the $Na_4Ca(PO_3)_6$ phase are seen to be disappeared. Also, the peaks of the $NaPO_3$ phase become lowered and new peaks of the $Na_5Ti(PO_4)_3$ phase are distinguished. This effect may be correlated with the assumption of the depolymerization effect of TiO_2 on the metaphosphate network [11].

The depolymerization of the metaphosphate by TiO_2 is also reflected on the infrared absorption spectra of the phosphate glasses. The incorporation of titanium into a new crystalline phase does not inhibit the decrease of sodium metaphosphate $NaPO_3$ phase except in sample P5. The X-ray diffraction pattern of sample P5 reveals that the peaks of the $NaPO_3$ phase are still high. The new titanium phase in sample P5 possesses also high intensity peaks which, indicate that titanium is consumed nearly inside this phase. So, the $NaPO_3$ phase is shown to increase again.

The images of the scanning electron microscope (Fig. 5) show that the addition of TiO_2 results in the observed morphological structure variations between the samples. These results indicate that TiO_2 has a pronounced effect on the nucleation and crystallization processes [10,11] because the addition of even small quantities of TiO_2 to the base glass results in obvious variation of the surface texture. X-ray diffraction results indicate the effect of TiO_2 on the crystalline phases formed in the glass–ceramics which is reflected on the surface texture of the samples. By increasing the TiO_2 content, the intensities of the precipitated crystalline phases change, where the $NaPO_3$ and β-Ca $(PO_3)_2$ phases decrease whereas the $Na_4P_2O_7$ and $Na_4Ca(PO_3)_6$ phases nearly disappear and a new $Na_5Ti(PO_4)_3$ phase is resolved.

4.3. Corrosion studies

First, it can be assumed that the dissolution of the phosphate glasses must be considered to explain the behavior of the glassy phase and the crystalline phosphate phases as well towards the action of aqueous solutions (i.e. SBF). Bunker et al. [17] showed that the phosphate glass dissolves congruently or uniformly which means that the dissolution products in the solution have identical composition with that of the bulk glass. The dissolution process is believed to be divided into two kinetic periods according to the profiles of dissolved amount, q vs. time, t, e.g., a decelerating dissolution period of $q \propto t^{1/2}$ and a uniform dissolution period of $q \propto t$. They also showed that the hydrolysis of the linear polymeric phosphates exhibits clear pH dependence. Hydrolysis is believed to be accelerated in acids, with a fractional dependence on $[H^+]$.

Phosphate glasses dissolve in aqueous media in the following two interdependent steps [18]:

(1) Hydration reaction: the glass exchanges its sodium ions with the hydrogen ions in water to carry out Na–H ion exchange reaction, resulting in the formation of a hydrated layer on the glass surface at the glass–water interface.
(2) Network breakage: under the attack of hydrogen ions and water molecules, the P–O–P bonds in hydrated layer break up and result in the destruction of the glass network and the release of chains of phosphates with different degree of polymerization into the solution.

The glass–ceramic samples are known to consist of both crystalline phases and residual glassy phase. The corrosion of such glass–ceramic samples can be explained by considering the solubility properties of both the crystalline phases and the glassy phase. Lin et al. [19] studied the degradation of β-$Ca_2P_2O_7$ in distilled water and found that it is stable and inert. Antonucci et al. [20] reported that calcium metaphosphate (β-$Ca(PO_3)_2$) is extremely insoluble in aqueous solutions, even in acidified aqueous media. On the other hand, $NaPO_3$ and $Na_4P_2O_7$ were reported to dissolve easily in aqueous media [21]. The quite high chemical durability of calcium metaphosphate phase can be explained by considering its structure. For β-$Ca(PO_3)_2$, the polymeric structure shows the covalently bound PO_3 units which are structurally linked through P–O–P bonds to form long metaphosphate chains. These chains are ionically bound to calcium between chains. Therefore, the divalent cations can serve as ionic cross-links between the nonbridging oxygens of two different chains. The formation of such cross-links explains the quite high chemical durability.

The X-ray diffraction data are known to provide accurate information of the crystalline phases and their evolution inside the glass–ceramic samples. Using these data and the solubility properties of the different phases, the degradation behavior of the glass–ceramic samples can thus be understood and explained. It is obvious that the effective crystalline phase in the dissolution process is $NaPO_3$ phase because it is found in all the samples with considerable amounts (as seen from X-ray diffraction data). Also, the residual glassy phase must be taken into consideration.

From careful inspection of the phosphorous ions release from the phosphate bioglass–ceramic samples shown in Fig. 6, it is evident the fast release of the phosphorous ions at the early times of immersion which indicates that the sodium metaphosphate crystalline phase and the residual glassy phase found on

the surface are expected to dissolve rapidly into the SBF solution. Also, it is obvious that the release of phosphorous ions from the samples P1 and P5 are the highest. This can be explained by considering the crystalline phases composition of the samples which are revealed by X-ray diffraction measurements. The high release of phosphorous ions from sample P1 is due to the absence of titanium, so the sodium metaphosphate $NaPO_3$ crystalline phase is formed with high amount. Also, the X-ray diffraction results show that the relative amount of the sodium metaphosphate $NaPO_3$ crystalline phase in sample P5 is higher than that of the rest of the samples containing titanium. Thus, the increase of the sodium metaphosphate phase obviously results in the increase of the release of the phosphorous ions from sample P5.

Fig. 7 reveals the progressive increase of the released sodium ions from the samples which indicates that the crystalline phases containing sodium ions seem to dissolve constantly. Also the data of the release of calcium ions (Fig. 8) indicate that the calcium ions may be released at the beginning from the residual glassy phase then is assumed to reach to a maximum quantity.

4.4. In vitro measurements of bioglass–ceramic samples

4.4.1. Surface analysis using infrared reflection spectroscopy

Figs. 9 and 10 before immersion in SBF solution reveal the existence of metaphosphate and pyrophosphate units on the surfaces of the samples as indicated by the presence of the following IR reflection peaks [12]:

(a) The peaks at 1320 cm^{-1} and 1275 cm^{-1} are assigned as PO_2 asymmetric stretching vibration modes.
(b) The shoulder at 1158 cm^{-1} is assigned as PO_2 symmetric stretching vibration.
(c) The peak at 1103 cm^{-1} is assigned as PO_3 asymmetric stretching vibration.
(d) The peak at 1022 cm^{-1} is assigned as PO_3 symmetric stretching vibration.
(e) The peak at 893 cm^{-1} is due to asymmetric stretching vibration of P–O–P groups.
(f) The doublet peaks at 774 cm^{-1} and 742 cm^{-1} are assigned as symmetric stretching vibration of P–O–P group.
(g) The peaks at 666 cm^{-1} and 515 cm^{-1} are assigned as the bending vibration of P–O bonds [22].

After the immersion in SBF solution, the intensities of the characteristic peaks of metaphosphate units are shown to decrease with time and all the IR spectra are converted after 14 days immersion in SBF solution, into the characteristic spectrum of calcium pyrophosphate (β-$Ca_2P_2O_7$) [23], which is seen to be the main crystalline phase in the phosphate bioglass–ceramic samples as indicated by X-ray diffraction measurements. This conversion is also verified by the following changes:

(a) The disappearance of the characteristic peaks of metaphosphate chains (PO_2 asymmetric stretching vibration) which are located at 1320 cm^{-1} and 1275 cm^{-1} [12]
(b) The appearance of strong peak at 560 cm^{-1} (bending vibration of P–O bonds), which is characteristic peak of calcium pyrophosphate [23].
(c) The decrease of the peak at 775 cm^{-1}, which is characteristic of the metaphosphate compositions (symmetric stretching vibration of P–O–P group) [12].

However, the conversion of the reflection spectra into the characteristic spectrum of calcium pyrophosphate did not occur at the same time. The samples P1 and P2 are the fastest in this conversion. The appearance of the characteristic spectrum of calcium pyrophosphate for samples P1 and P2 occurred after 3 days immersion in SBF solution while for samples P3, P5, and P6, after 7 days and for sample P4, after 14 days.

4.5. Surface analysis using scanning electron microscope

The scanning electron micrographs (Fig. 11) indicate that the texture of the surface for all the phosphate bioglass–ceramic samples exhibit the same features and characteristics. Surface analysis by infrared reflection spectroscopy indicates the crystalline calcium pyrophosphate phase to be the main phase found on the surfaces after 14 days immersion in SBF solution. There is no any indication for the presence of the apatite layer on the surface of the samples.

5. Conclusion

The bioactivity of some bioglass–ceramics from the system Na_2O–CaO–P_2O_5 before and after the addition of few percents of TiO_2 was studied. X-ray diffraction patterns of the crystalline phases indicated that calcium pyrophosphate, sodium pyrophosphate, calcium metaphosphate, sodium metaphosphate together with sodium titanium phosphate were formed after two-step heat treatment of the parent bioglasses. The results showed that no apatite surface layer was formed during the immersion in SBF and the dominant phase remained on the glass–ceramics surface was bioactive calcium pyrophosphate.

References

[1] L.L. Hench, J. Am. Ceram. Soc. 81 (1998) 1705–1728.
[2] T. Kokubo, J. Non-Cryst. Solids 120 (1990) 138–151.
[3] T. Kitsugi, T. Yamamuro, T. Nakamura, S. Kotani, T. Kokubo, H. Takeuchi, Biomaterials 14 (1993) 216–224.
[4] W. Vogel, W. Holand, Angew. Chem. Int. 26 (1987) 527–544.
[5] J. Alkemper, H. Fuess, J. Non-Cryst. Solids 210 (1997) 32–40.
[6] M. Uo, M. Mizuno, Y. Kuboki, A. Makishima, F. Watari, Biomaterials 19 (1998) 2277–2284.
[7] T. Kasuga, M. Sawada, M. Nogami, Y. Abe, Biomaterials 20 (1999) 1415–1420.
[8] T. Kasuga, Y. Hosoi, M. Nogami, M. Niinomi, J. Am. Ceram. Soc. 84 (2001) 450–452.
[9] T. Kokubo, H. Kushitani, S. Sakka, T. Kitsugi, T. Yamamuro, J. Biomed. Mater. Res. 24 (1990) 721–734.
[10] R.K. Brow, D.R. Tallant, W.L. Warren, A. McIntyre, D.E. Day, Phys. Chem. Glasses 38 (1997) 300–306.
[11] L. Koudelka, P. Mosner, M. Zeyer, C. Jager, J. Non-Cryst. Solids 326&327 (2003) 72–76.

[12] A. Shaim, M. Et-tabirou, L. Montagne, G. Palavit, Mater. Res. Bull. 37 (2002) 2459–2466.
[13] I. Abrahams, G.E. Hawkes, J.C. Knowles, J. Chem. Soc.: Dalton Trans. (1997) 1483–1484.
[14] Y. Zhang, J.D. Santos, J. Non-Cryst. Solids 272 (2000) 14–21.
[15] P. Hartmann, J. Vogel, B. Schnabel, J. Non-Cryst. Solids 176 (1994) 157–163.
[16] K. Franks, I. Abrahams, J.C. Knowles, J. Mater. Sci.: Mater. Med. 11 (2000) 609–614.
[17] B.C. Bunker, G.W. Arnold, J.A. Wilder, J. Non-Cryst. Solids 64 (1984) 291–316.
[18] H. Gao, T. Tan, D. Wang, J. Control. Release 96 (2004) 29–36.
[19] F.-H. Lin, C.-J. Liao, K.S. Chen, J.-S. Sun, H.-C. Liu, Biomaterials 18 (1997) 915–921.
[20] J.M. Antonucci, B.O. Fowler, S. Venz, Dent. Mater. 7 (1991) 124–129.
[21] D.R. Lide, CRC Handbook of Physics and Chemistry, CRC Press, Boca Raton, 2004.
[22] A. Aronne, L.E. Depero, V.N. Sigaev, P. Pernice, E. Bontempi, O.V. Akimova, E. Fanelli, J. Non-Cryst. Solids 324 (2003) 208–219.
[23] D. de Waal, C. Hutter, Mater. Res. Bull. 29 (1994) 1129–1135.